Renewable Energy 219 (2023) 119523

Contents lists available at ScienceDirect

Renewable Energy

journal homepage: www.elsevier.com/locate/renene

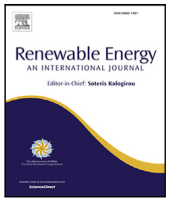

Control co-design of power take-off and bypass valve for OWC-based wave energy conversion systems

Marco Rosati *, John V. Ringwood

Centre for Ocean Energy Research (COER), Maynooth University, Co. Kildare, Ireland

ARTICLE INFO

Keywords:
Bypass valve
Control co-design
Levelised cost of energy
Oscillating-water-column
Wave energy
Wells turbine

ABSTRACT

Wave energy is a significant source of renewable energy harnessed by wave energy converters (WECs). However, due to the relatively high levelised cost of energy (LCoE), wave energy has not attained a commercial stage yet. To minimise the LCoE, since the optimum (uncontrolled) WEC design typically differs from the optimum controlled WEC design, control co-design (CCD) techniques are essential. With CCD, the WEC control-related aspects are taken into account from the start of the WEC design phase and, ideally, the best *control-informed* WEC design is then achieved. This paper specifically focuses on CCD for an oscillating-water-column (OWC) WEC, equipped with a Wells turbine and a bypass valve. In essence, a parametric CCD approach is devised to find the optimum (control-informed) turbine rotor diameter, and bypass valve diameter, for the considered OWC WEC. In particular, the optimum design parameters minimise a 'simplified' LCoE, which is chosen as a suitable performance function. Despite the LCoE is primarily sensitive to the power take-off size, rather than to the bypass valve size, peak-shaving control with a bypass valve potentially increases the capacity factor and, consequently, can minimise the LCoE for small-to-medium sized turbines.

1. Introduction

Wave energy, harnessed by wave energy converters (WECs), is an almost untapped renewable energy source, with an estimated global potential around 16 000–18 500 TWh/year [1], which can significantly contribute to decarbonisation [2]. Furthermore, the diversification of renewable energy sources [3] is imperative to achieve a reliable renewable energy supply. It is therefore important to note the relatively good complementarity (i.e., poor correlation) between wave and other renewable resources [4,5], meaning that the integration of wave energy in the renewable mix can effectively reduce variability in electrical power production.

The oscillating-water-column (OWC) [6], shown in Fig. 1, is one of the most promising WECs, particularly since all the moving parts are above the water level. Furthermore, in comparison with other WECs, a significant advantage of the OWC is the possibility to easily dissipate excessive power using a bypass valve [7,8]. The OWC operating principle is straightforward. A water column, excited by the incoming ocean waves, alternatively compresses/decompresses an air volume in a pneumatic chamber. The air compression/expansion process causes a bidirectional airflow, typically utilised to drive a self-rectifying air turbine [9], such as a Wells or an impulse-like turbine. To avoid a catastrophic system failure due to turbine overspeeding, a safety (shut-off) valve is normally installed [10,11]. Finally, a suitable electric generator [12], directly coupled with the turbine, converts the turbine mechanical power into electrical power.

To date, WECs struggle to penetrate the renewable energy market due to the high levelised cost of energy (LCoE) characterising wave energy projects [2] (onshore/nearshore plants: LCoE ≈ 123 $/MWh; offshore farms: LCoE ≈ 359 $/MWh), in comparison with the main alternatives [2,13] (offshore wind: LCoE ≈ 109 $/MWh; onshore wind: LCoE ≈ 72.5 $/MWh; tidal: LCoE ≈ 203.5 $/MWh). If CapEx and OpEx are, respectively, the capital and operational costs, the LCoE is written as

$$\mathrm{LCoE} = \frac{\mathrm{CapEx} + \mathrm{OpEx}}{\text{Produced energy over the WEC lifetime}}. \tag{1}$$

To minimise the LCoE, high-performance energy maximising control strategies are vital [14] and, to this end, since the WEC geometry optimisation problem is coupled with the WEC control problem [15,16], *control co-design* (CCD) [17,18] techniques are crucial to achieve the optimum control-informed WEC design [16,19–21]. In a traditional design approach, design is a progressive stepwise procedure in which control aspects are not considered until a late stage. Furthermore, in traditional design, the design choices made at each step reduce the design possibilities of the next step [22]. In other words, each step limits the design flexibility of the next step, making a design change increasingly difficult and expensive. In CCD, control aspects

* Corresponding author.
E-mail addresses: marco.rosati.2021@mumail.ie (M. Rosati), john.ringwood@mu.ie (J.V. Ringwood).

https://doi.org/10.1016/j.renene.2023.119523
Received 28 June 2023; Received in revised form 2 October 2023; Accepted 25 October 2023
Available online 27 October 2023

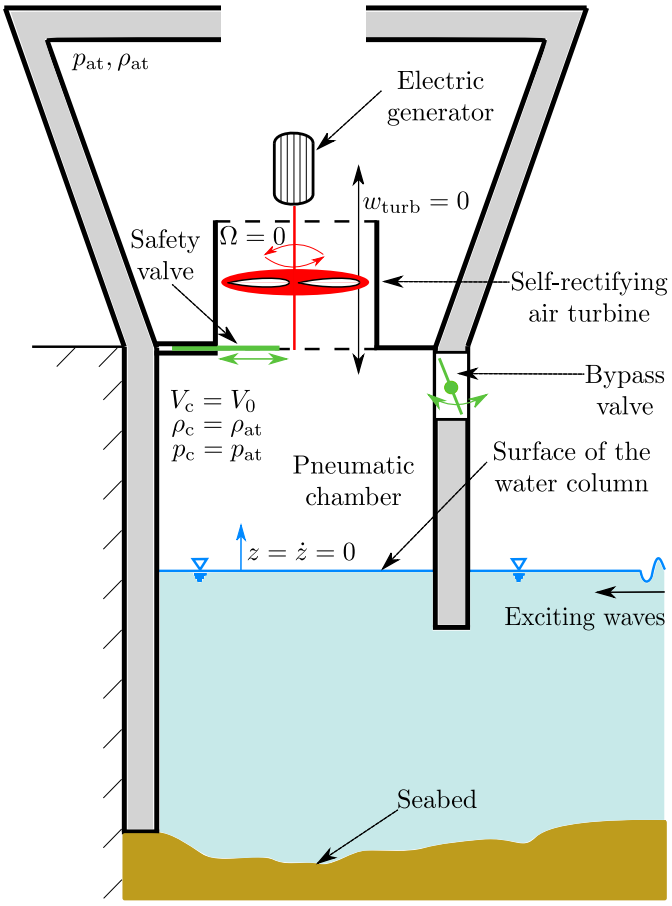

Fig. 1. Schematic of a fixed OWC WEC, equipped with a Wells turbine, a bypass valve, and a safety valve, in still water conditions.
Source: Adapted from [23].

are considered from an initial design phase, potentially improving control-awareness and flexibility in overall design optimisation [22].

In this paper, a parametric CCD approach is devised to optimise the Wells turbine rotor, and bypass valve diameters, for a Mutriku-like OWC system [24]. The optimum system parameters minimise a 'simplified LCoE', which is selected as a suitable performance function. For each possible combination in the parametric space, suitable strategies for controlling the turbine rotational speed (Section 3.3.1) the bypass valve position (Section 3.3.2), and the safety valve position (Section 3.3.3), are designed. In general, a comprehensive OWC control strategy [10,25] should focus on: (i) Turbine rotational speed control, for maximising the OWC (overall) *wave-to-wire* (W2W) efficiency [23,26,27]; (ii) peak-shaving control [25], for increasing the *capacity factor*, defined as

$$\text{Capacity factor} = \frac{\text{Produced time-averaged power}}{\text{Rated power}}, \tag{2}$$

when the available wave power is sufficiently high. In a relatively high-energy sea state (SS), peak-shaving (or rated power) control is key to extend the OWC operational range by somewhat limiting the available/converted pneumatic power [25]; otherwise, to avoid a system failure, the OWC must enter a safety mode by closing the safety valve, which discontinues pneumatic excitation of the turbine. To date, OWC peak-shaving control has received very little attention, particularly for Wells turbines. In radial-flow impulse turbines, wave-by-wave peak-shaving control can be implemented in real-time, thanks to a small in-series valve [28,29]. With a Wells turbine, peak-shaving can be achieved by partially opening a bypass valve [7,8] to dissipate excessive pneumatic power. However, even using wave forecasting techniques [30,31], wave-by-wave bypass valve control is difficult to implement in real-time, due to the low valve actuation speed [32] with respect to the wave celerity. Therefore, in this paper, a sea state based (SS-based) controller for the bypass valve position is proposed. With SS-based bypass valve control, the position of the bypass valve essentially depends on the SS or, equivalently, on the available wave power.

The main contributions of this paper are summarised in three points:

1. A parametric CCD approach, for an OWC with a bypass valve and a Wells turbine, is devised;
2. a novel, SS-based, bypass valve position controller for increasing the capacity factor is proposed;
3. the impact of peak-shaving control on the capacity factor, and LCoE, is analysed.

The reminder of the paper is structured as follows. Section 2 provides a W2W model for the considered OWC system. In Section 3, the proposed CCD approach is detailed. Finally, results are discussed in Section 4 and conclusions are drawn in Section 5.

2. OWC system modelling

This section provides a W2W model for the Mutriku-like OWC considered in this paper. The W2W power flow for the considered OWC system is shown in Fig. 2. Throughout this section, the time dependence of variables is omitted to simplify the notation.

2.1. Hydrodynamic modelling

If the water column is modelled as a neutrally buoyant piston, under linear potential theory assumptions, the hydrodynamic model of a fixed OWC is written [33] as

$$m_p \dot{v} = -\rho_w g S_w z - S_w p_c - f_r + f_{ex}, \tag{3}$$

where z is the water column position relative to the still water level, $v = \dot{z}$ is the water column velocity, m_p is the piston mass, S_w is the water plane area, p_c is the air chamber pressure, ρ_w is the water density, and g is the gravity acceleration constant. Furthermore, f_{ex} and f_r are, respectively, the excitation force due to incident waves of frequency ω, and the force due to radiated waves, written as

$$f_r = A(\infty)\dot{v} + \int_{-\infty}^{t} k_r(t-\tau)\, v(\tau)\, d\tau, \tag{4}$$

where k_r is the piston impulse response function, computed as the inverse Fourier transform of the OWC radiation damping, $B(\omega)$, while $A(\infty)$ is the OWC added mass at infinite frequency ($A(\omega)|_{\omega\to\infty} = A(\infty)$). Finally, f_{ex} is computed as a sum of N frequency components ω_n [11], as

$$f_{ex} = \sum_{n=1}^{N} A_n \cos(\omega_n t + \phi_n), \tag{5}$$

where A_n and ϕ_n are, respectively, the sets of discrete amplitudes and phases of f_{ex}. A boundary element problem is solved [34], using the WAMIT software [35], to find the frequency dependent functions $A(\omega)$, $B(\omega)$, $A_n(\omega)$, and $\phi_n(\omega)$. A complete description of the frequency dependant parameters considered in this paper can be found in [11].

It is common practice, in the wave energy field, to approximate the convolution integral in Eq. (4) with a suitable, and more computationally efficient, linear state space model [36]. To this end, Prony's method [36] is used.

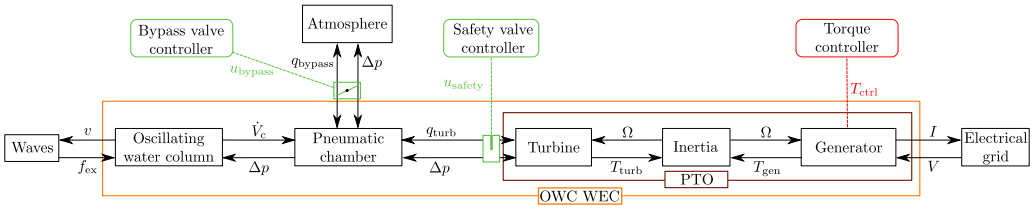

Fig. 2. Wave-to-wire power flow of the OWC system considered in this paper.
Source: Adapted from [25].

2.2. Air chamber modelling

The air chamber pressure, p_{c}, is modelled [11] as

$$\frac{\dot{p}_{\text{c}}}{p_{\text{c}}} = -\frac{\gamma}{V_{\text{c}}}\left(\dot{V}_{\text{c}} + \frac{w_{\text{turb}} - w_{\text{bypass}}}{\rho_{\text{c}}}\right), \tag{6}$$

where $V_{\text{c}} = V_0 - S_{\text{w}} z$ is the volume of air (with V_0 being the air volume in still water), γ is the air specific heat ratio, w_{turb} indicates the turbine air mass flow rate (positive for outward flow), and w_{bypass},

$$w_{\text{bypass}} = \text{sgn}(\Delta p) C_{\text{d}} A_{\text{bypass}}(u_{\text{bypass}}) \sqrt{2\rho_{\text{air}} \Delta p}, \tag{7}$$

is the bypass air mass flow rate. In Eq. (7), $C_{\text{d}} = 0.6$ [37] is the discharge coefficient, $\Delta p = p_{\text{c}} - p_{\text{at}}$, and $A_{\text{bypass}} = u_{\text{bypass}}(\pi d_{\text{bypass}}^2/4)$ is the bypass area, with u_{bypass} the bypass valve position and d_{bypass} the bypass valve diameter. If the air compression/expansion process is isentropic, the air chamber density [38] is

$$\rho_{\text{c}} = \rho_{\text{at}} \left(\frac{p_{\text{c}}}{p_{\text{at}}}\right)^{1/\gamma}, \tag{8}$$

where the subscript 'at' refers to standard atmosphere values. Finally, the pneumatic power available to the turbine is written as $P_{\text{pneu}} = \Delta p\, q_{\text{turb}}$, while the pneumatic power dissipated through the bypass valve is computed as $P_{\text{bypass}} = \Delta p\, q_{\text{bypass}}$. The terms $q_{\text{turb}} = w_{\text{turb}}/\rho_{\text{air}}$ and $q_{\text{bypass}} = w_{\text{bypass}}/\rho_{\text{air}}$ indicate, respectively, the turbine air volume flow rate and the bypass air volume flow rate.

2.3. PTO system modelling

The PTO system model [10], if bearing friction losses are ignored, is

$$\frac{\text{d}}{\text{d}t}\left(\frac{1}{2} I \Omega^2\right) = P_{\text{turb}} - T_{\text{ctrl}}\, \Omega, \tag{9}$$

where Ω is the turbine rotational speed, I is the inertia moment, P_{turb} is the turbine power, and T_{ctrl} is the generator control torque.

Furthermore, if the Mach number is small and the Reynolds number is large, the turbine can be modelled using the following dimensionless functions [39]

$$\Phi = f_{\Phi}(u_{\text{safety}}\Psi),\ \Pi = f_{\Pi}(u_{\text{safety}}\Psi). \tag{10}$$

In Eq. (10), u_{safety} is the safety valve position (closed: $u_{\text{safety}} = 0$, open: $u_{\text{safety}} = 1$), whereas Φ, Π, and Ψ, defined as

$$\Phi = \frac{w_{\text{turb}}}{\rho_{\text{air}}\, \Omega\, d_{\text{r}}^3},\ \Pi = \frac{P_{\text{turb}}}{\rho_{\text{air}}\, \Omega^3\, d_{\text{r}}^5},\ \Psi = \frac{\Delta p}{\rho_{\text{air}}\, \Omega^2\, d_{\text{r}}^2}. \tag{11}$$

are, respectively, the dimensionless mass flow rate, dimensionless turbine power, and dimensionless pressure head. The Wells turbine model considered in this paper is shown in Fig. 3. It should be noted that the Wells turbine damping, defined as

$$\Theta = \frac{w_{\text{turb}}}{\Delta p} = \frac{d_{\text{r}}}{\kappa\, \Omega}, \tag{12}$$

is a function of Ω, meaning that Wells turbine rotational speed affects the OWC hydrodynamic performance [23,40]. In Eq. (12), κ is a geometric constant.

Finally, for electric power calculation, the dimensionless generator efficiency map, shown in Fig. 4, is used [41] .

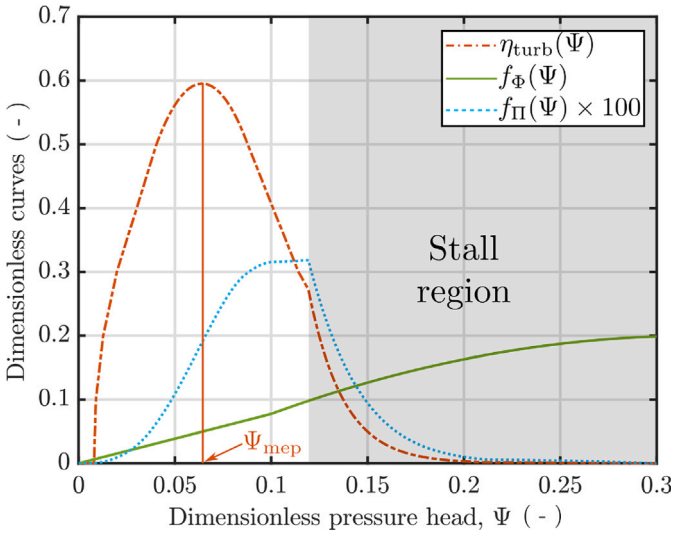

Fig. 3. Dimensionless flow rate, Φ, dimensionless power, Π, and turbine efficiency, η_{turb}, as functions of the dimensionless pressure head, Ψ, for the Wells turbine considered in this paper. Ψ_{mep} is the value of Ψ at the turbine maximum efficiency point (MEP). The grey shaded area represents the turbine stall region.
Source: Adapted from [23].

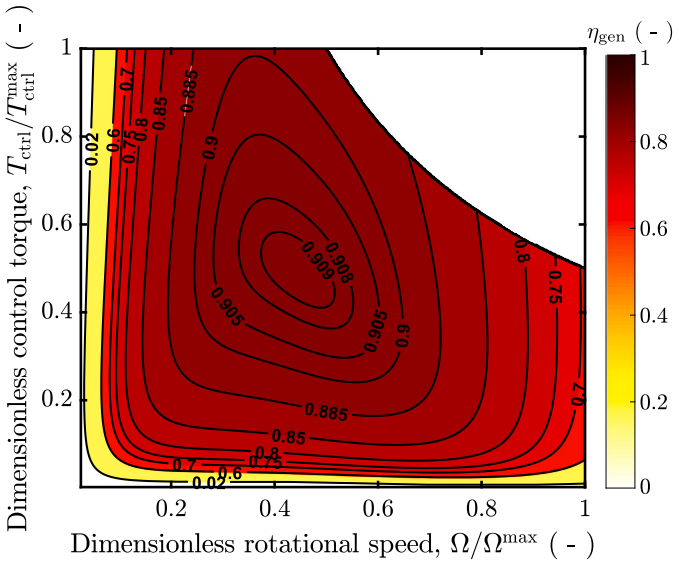

Fig. 4. Electric generator efficiency, η_{gen}, as a function of the dimensionless rotational speed, $\Omega/\Omega^{\max}$, and the dimensionless control torque, $T_{\text{ctrl}}/T_{\text{ctrl}}^{\max}$. $\Omega^{\max}$ and $T_{\text{ctrl}}^{\max}$ are, respectively, the maximum allowable rotational speed and the maximum control torque.
Source: Adapted from [41].

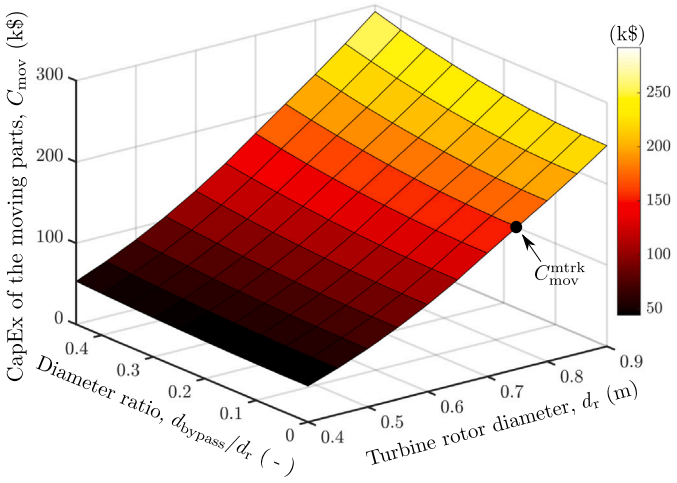

Fig. 5. Cost of the moving parts, C_{mov}, as a function of the turbine rotor diameter, d_r, and the ratio between bypass valve diameter and turbine rotor diameter, d_{bypass}/d_r. C_{mov}^{mtrk} is the cost of the moving parts of Mutriku OWC ($d_r = 0.75$ m, $d_{bypass}/d_r = 0$).

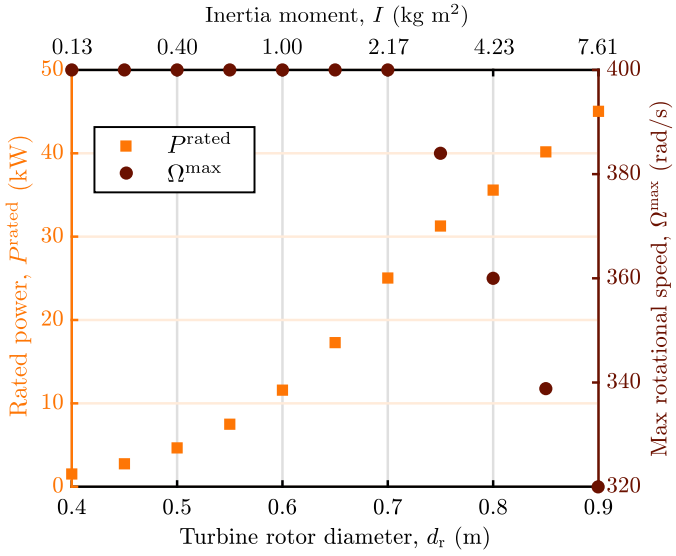

Fig. 6. Maximum rotational speed, Ω^{max}, PTO rated power, P^{rated}, and turbine inertia (top x-axis label), I, as functions of the turbine rotor diameter, d_r. If $d_r > 0.7$ m, $\Omega^{max} = \Omega_{turb}^{max}$, whereas if $d_r \leq 0.7$ m, $\Omega^{max} = \Omega_{gen}^{max}$.

3. Control co-design

In this section, the parametric CCD approach is devised. First, a suitable performance function is selected (Section 3.1) and the design parameters are specified (Section 3.2). Furthermore, control system design is addressed (Section 3.3) and, finally, the methodology is explained (Section 3.4).

3.1. Performance function selection

The 'complete' LCoE in Eq. (1) is, as a performance objective, difficult, especially due to the challenging estimation of OpEx. Therefore, a 'simplified' LCoE, denoted LCoE*, is adopted as a suitable performance function.

In this paper, since design variations in the PTO, and bypass valve, primarily affect CapEx and energy production, OpEx is simplified as a proportion of CapEx (OpEx = b CapEx, $0 \leq b \leq 1$). Furthermore, although OpEx depends, to some extent, on the control action [42], the control impact on OpEx is not expected to change significantly for the considered control approach (Section 3.3).

CapEx is written as CapEx = $C_{str} + C_{mov}$, where C_{str} is the OWC structure cost and C_{mov} (see Fig. 5), specified as

$$C_{mov}(d_r, d_{bypass}) = C_{pto}(d_r) + \mu(C_{safety}(d_r) + C_{bypass}(d_{bypass})), \tag{13}$$

is the cost of the moving parts, with

$$C_{pto}(d_r) = C_{mech}(d_r) + C_{elec}(d_r). \tag{14}$$

In Eqs. (13) and (14), C_{safety} is the safety valve material cost, C_{bypass} is the bypass valve material cost, μ is the manufacturing cost factor of the valves, C_{pto} is the PTO material and manufacturing cost, C_{mech} is the cost of the mechanical components, and C_{elec} is the cost of the electric generator and ancillary components. If geometric similarity for all the mechanical components is assumed, the mass of the material scales as d_r^3 and, therefore, $C_{mech} \propto d_r^3$. In particular, C_{mech} (in k$) is estimated [43], as

$$C_{mech}(d_r) = C_{mech}^{pico} \left(\frac{d_r}{d_r^{pico}} \right)^{\beta}, \tag{15}$$

where the empirical coefficients, C_{mech}^{pico} and β, are set from experience with the Pico power plant [32], while d_r^{pico} is the Pico turbine rotor diameter. Furthermore, C_{elec} (in k$) is computed [43], as

$$C_{elec}(d_r) = 3.026\,(P^{rated}(d_r))^{0.7}, \tag{16}$$

where P^{rated} (in kW) is the generator rated power. Since the safety valve diameter is approximately equal to d_r, C_{safety} is written as

$$C_{safety}(d_r) = \rho_{steel} \frac{\pi d_r^2}{4} t_h C_{steel}, \tag{17}$$

where t_h is the safety valve thickness, ρ_{steel} is the steel density, and C_{steel} is the cost per unit mass of steel. To compute C_{bypass}, d_r is replaced by d_{bypass} in Eq. (17). In Fig. 5, since d_{bypass} somewhat depends on d_r (indeed, the required power dissipation is a function of the PTO size), d_{bypass} is specified as a ratio between the diameters, d_{bypass}/d_r.

In this paper, C_{str} is constant, since the air chamber volume is fixed. It is assumed that C_{str} is a proportion of C_{mov} for the Mutriku OWC (i.e., $d_{bypass}/d_r = 0$ and $d_r = 0.75$ m), indicated as C_{mov}^{mtrk}. Therefore,

$$C_{str} = \varepsilon\, C_{mov}^{mtrk}, \tag{18}$$

where $\varepsilon > 1$.

Finally, applying the simplifications introduced so far in Section 3.1, LCoE* is written as

$$\text{LCoE}^* = (1+b)\,\frac{\varepsilon\, C_{mov}^{mtrk} + C_{mov}}{E_{elec}^{life}} = (1+b)\,\overline{\text{LCoE}}^*, \tag{19}$$

where E_{elec}^{life} is the produced electrical energy over the OWC lifetime. Ultimately, the CCD performance objective is to minimise $\overline{\text{LCoE}}^*$, as $(1 + b)$ is merely a multiplicative coefficient.

3.2. PTO and bypass valve specifications

As shown in Fig. 6, the PTO characteristics/limitations are solely functions of d_r. First, from geometric similarity, and assuming the same turbine rotor material, $I \propto d_r^5$, [11] as

$$\frac{I}{I^{mtrk}} = \left(\frac{d_r}{d_r^{mtrk}} \right)^5, \tag{20}$$

where I^{mtrk} and d_r^{mtrk} are, respectively, the PTO inertia moment and the turbine rotor diameter at Mutriku. Secondly, the maximum rotational speed [10] is specified as

$$\Omega^{max} = \min(\Omega_{gen}^{max}, \Omega_{turb}^{max}), \tag{21}$$

where Ω_{gen}^{max} (which is set at 400 rad/s [11,12]) is the maximum generator speed to limit centrifugal stresses, while Ω_{turb}^{max} is the turbine

maximum speed to avoid air compressibility effects (e.g., shock waves) at the rotor blade tips. If a maximum blade tip speed of 160 m/s is assumed [11], $\Omega_{\text{turb}}^{\max} = 160(2/d_{\text{r}})$. In general, Ω may also be limited to reduce turbine noise emission [44,45]. Without loss of generality, the generator rated power, P^{rated}, can be computed as the turbine power output when $\Psi = \Psi_{\text{mep}}$ and $\Omega = \Omega^{\max}$. Finally, the maximum allowable control torque, $T_{\text{ctrl}}^{\max}$, is derived from $\Omega^{\max}$ and P^{rated} [11], as

$$T_{\text{ctrl}}^{\max} = 2.266 \frac{P^{\text{rated}}}{\Omega^{\max}}. \tag{22}$$

The range of values for d_{r} is established considering the Wells turbine rotor diameter at Mutriku ($d_{\text{r}}^{\text{mtrk}} = 0.75$ m) as an initial guess, and reasonable PTO limits. The upper bound ($d_{\text{r}} = 0.90$ m) is motivated by the fact that, if $d_{\text{r}} > 0.90$ m, P^{rated} is large enough to allow wave energy extraction in high energy sea states, even without a bypass valve (therefore, power dissipation is not needed). Furthermore, to operate close to the turbine maximum efficiency point ($\Psi = \Psi_{\text{mep}}$), Ω should increase as d_{r} decreases. However, if $d_{\text{r}} < 0.40$ m, since Ω cannot exceed $\Omega^{\max}(= \Omega_{\text{gen}}^{\max})$, the turbine operates at very low efficiency and, inevitably, the produced energy drops.

The initial guess for $d_{\text{bypass}}/d_{\text{r}}$ is inspired by the Pico bypass valve (equivalent) diameter [32], $d_{\text{bypass}}^{\text{pico}}$. Since u_{bypass} is SS-based (and not controlled wave-by-wave), the bypass valve (if open) provides continuous pneumatic power dissipation. It should be noted that the Pico bypass valve was not optimised for SS-based control. Therefore, the optimum $d_{\text{bypass}}/d_{\text{r}}$ for SS-based bypass valve control is likely to be smaller than $d_{\text{bypass}}^{\text{pico}}/d_{\text{r}}^{\text{pico}} \approx 0.6$. Ultimately, $d_{\text{bypass}}/d_{\text{r}} = 0.3$ is adopted as the initial guess for $d_{\text{bypass}}/d_{\text{r}}$, while the upper and lower bounds are, respectively, 0.45 and 0 (i.e., no bypass valve).

3.3. Control system design

The OWC system modelled in Section 2 has three manipulated inputs: T_{ctrl}, u_{bypass}, and u_{safety}. In this section, a low-level rotational speed controller, using T_{ctrl}, and suitable high-level valve position controllers, using u_{bypass} and u_{safety}, are designed.

3.3.1. Rotational speed control

Since the Wells turbine rotational speed affects the OWC hydrodynamic performance, Wells turbine rotational speed control should focus on maximising the OWC W2W efficiency [23,27], though the majority of OWC control strategies in the literature focus on a simplified control objective, namely turbine efficiency maximisation [11,25,46–48]. For a Wells turbine, a possible W2W efficiency maximising (steady-state) control law has the following form [23]:

$$T_{\text{ctrl}}^{\text{w2w}} = (l_1 + l_2\,\Omega + e_1\,\exp^{e_2\,\Omega})/\Omega, \tag{23}$$

where the free parameters, l_1, l_2, e_1, and e_2, are optimised, for each d_{r}, following the procedure detailed in [23]. Eq. (23) can be modified to take into account the PTO control constraints [11], as

$$T_{\text{ctrl}} = \min(T_{\text{ctrl}}^{\text{w2w}}, T_{\text{ctrl}}^{\max}, \frac{P^{\text{rated}}}{\Omega}). \tag{24}$$

To avoid exceeding P^{rated}, T_{ctrl} can be 'detuned' [11], as $T_{\text{ctrl}} = P^{\text{rated}}/\Omega < T_{\text{ctrl}}^{\text{w2w}}$, so that the OWC operates below the W2W peak efficiency. However, torque detuning leads to an increase in Ω and, eventually, $\Omega_{\max}$ is attained and the OWC enters safety mode. It should be noted that increasing the torque beyond $T_{\text{ctrl}}^{\text{w2w}}$ is not a viable torque detuning solution, as Ω decreases and the turbine may stall (accompanied by a high noise emission and a risk of damaging the turbine). A possible way to limit safety valve actuation, but keep the OWC operational, is to use a bypass valve to dissipate excessive power. It should be noted that, for other WECs, due to the lack of suitable actuators, torque detuning is typically the only available control approach to reduce the power to the generator [e.g.,49].

3.3.2. Bypass valve position control

Peak-shaving control extends the range of sea states over which the OWC can retain power production operation. The bypass valve position, u_{bypass}, is set depending on the SS or, equally, on the mean wave power available to the OWC system, computed as

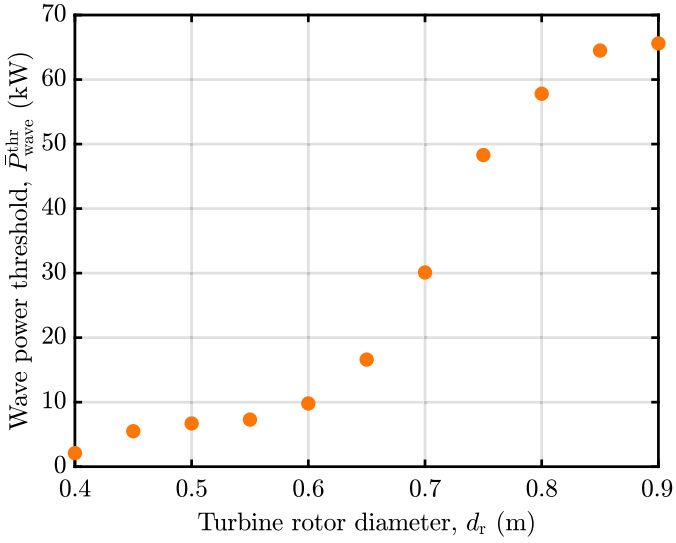

Fig. 7. Wave power threshold, $\bar{P}_{\text{wave}}^{\text{thr}}$, for each considered turbine rotor diameter, d_{r}.

$$\bar{P}_{\text{wave}} = \iota \hat{P}_{\text{wave}}, \tag{25}$$

where ι is the OWC capture width and $\hat{P}_{\text{wave}}$, which is a function of the sea state, is the time-averaged wave power per metre of wave crest. If $\bar{P}_{\text{wave}}$ is below a certain threshold value, $\bar{P}_{\text{wave}}^{\text{thr}}$, the bypass valve is closed ($u_{\text{bypass}} = 0$), as power dissipation is not required. If $\bar{P}_{\text{wave}}$ exceeds the maximum wave power for which the OWC can operate, $\bar{P}_{\text{wave}}^{\max}$, the bypass valve is fully open ($u_{\text{bypass}} = 1$). Finally, if $\bar{P}_{\text{wave}}^{\text{thr}} < \bar{P}_{\text{wave}} < \bar{P}_{\text{wave}}^{\max}$, $u_{\text{bypass}} = f_{\text{bypass}}(\bar{P}_{\text{wave}}^{*})$, where

$$\bar{P}_{\text{wave}}^{*} = \frac{\bar{P}_{\text{wave}} - \bar{P}_{\text{wave}}^{\text{thr}}}{\bar{P}_{\text{wave}}^{\max} - \bar{P}_{\text{wave}}^{\text{thr}}} \tag{26}$$

is the relative available wave power and $0 < f_{\text{bypass}}(\bar{P}_{\text{wave}}^{*}) < 1$. Ultimately, u_{bypass} is exclusively determined by choosing: (i) $\bar{P}_{\text{wave}}^{\text{thr}}$, (ii) $\bar{P}_{\text{wave}}^{\max}$, and (iii) $f_{\text{bypass}}(\bar{P}_{\text{wave}}^{*})$.

The value of $\bar{P}_{\text{wave}}^{\text{thr}}$, which is function of d_{r} (see Fig. 7), is selected so that the bypass valve opens only if power dissipation is needed. In other words, $\bar{P}_{\text{wave}}^{\text{thr}}$ is the wave power at which torque detuning alone is no longer sufficient to avoid exceeding $\Omega^{\max}$. In this paper, $\bar{P}_{\text{wave}}^{\max} = 265$ kW, which is selected considering the typical wave climate at Mutriku (see Section 3.4).

The simplest choice for the f_{bypass} function is a straight line, namely $f_{\text{bypass}}^{\text{line}} = \bar{P}_{\text{wave}}^{*}$, i.e., u_{bypass} is a linear function of $\bar{P}_{\text{wave}}^{*}$. However, $f_{\text{bypass}} = f_{\text{bypass}}^{\text{line}}$ may not be the ideal solution, since f_{bypass} should be designed considering: (i) How the time-averaged electrical power, $\bar{P}_{\text{elec}}$, increases with $\bar{P}_{\text{wave}}$ and (ii) how $\bar{P}_{\text{elec}}$ decreases as the bypass valve opens (i.e., as u_{bypass} varies from 0 to 1). Fig. 8(a) shows that, in an unconstrained control scenario, $\bar{P}_{\text{elec}}$ increases linearly with $\bar{P}_{\text{wave}}$, while Fig. 8(b) shows that $\bar{P}_{\text{elec}}$ decreases as $(u_{\text{bypass}}^{*})^{1.475}$. Therefore, if u_{bypass} is small, $\mathrm{d}\bar{P}_{\text{elec}}/\mathrm{d}u_{\text{bypass}}$ is smaller but, as u_{bypass} increases, $\bar{P}_{\text{elec}}$ decreases at a faster rate. This is arguably due to the fact that P_{pneu} strongly depends on Δp but, if u_{bypass} is small, the chamber pressure levels do not significantly decrease, resulting in little pneumatic power dissipation. In the light of these considerations, f_{bypass} is designed by 'mirroring' the dashed curve in Fig. 8(b) around the diagonal. In this way, for lower values of $\bar{P}_{\text{wave}}^{*}$ (< 0.45), f_{bypass} increases faster than $f_{\text{bypass}}^{\text{line}}$ and, for higher values of $\bar{P}_{\text{wave}}^{*}$ (> 0.45), f_{bypass} increases more slowly than $f_{\text{bypass}}^{\text{line}}$. In other words, since the electrical power increases linearly with the available wave power, the electrical power decrease, $\bar{P}_{\text{elec}}^{\text{decr}}$, should ideally be a linear function of u_{bypass} (which, however,

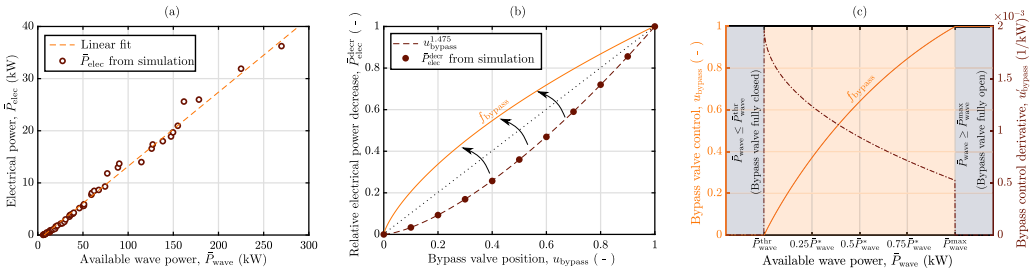

Fig. 8. Bypass valve control design. (a) Time-averaged electrical power, $\bar{P}_{elec}$, as a function of the available wave power, $\bar{P}_{wave}$. (b) Relative electrical power decrease, $\bar{P}_{elec}^{decr}(u_{bypass}) = (\bar{P}_{elec}(u_{bypass} = 0) - \bar{P}_{elec}(u_{bypass}))/(\bar{P}_{elec}(u_{bypass} = 0) - \bar{P}_{elec}(u_{bypass} = 1))$, as a function of the bypass valve position, u_{bypass}. (c) Bypass valve position controller, u_{bypass}, and its derivative $u'_{bypass} = du_{bypass}/d\bar{P}_{wave}$.

is not the case, as shown in Fig. 8(b)). As such, to compensate for the varying sensitivity of $\bar{P}_{elec}^{decr}$ to u_{bypass}, and therefore obtain a linear relationship between $\bar{P}_{elec}^{decr}$ and the available wave power, f_{bypass} is derived by the aforementioned mirroring procedure. Ultimately, with the resulting f_{bypass}, the bypass valve position is controlled in such a way that the power dissipation, due to the bypass valve opening, is a linear function of the available wave power.

Finally, Figs. 8(c) shows the complete u_{bypass} calculation, written as

$$u_{bypass} = \begin{cases} 0 & \text{if } \bar{P}_{wave} \leq \bar{P}_{wave}^{thr}, \\ 1 & \text{if } \bar{P}_{wave} \geq \bar{P}_{wave}^{max}, \\ f_{bypass} & \text{else,} \end{cases} \tag{27}$$

where,

$$f_{bypass} = 2\bar{P}_{wave}^{*} - (\bar{P}_{wave}^{*})^{1.475}. \tag{28}$$

3.3.3. Safety valve position control

To avoid turbine rotor disintegration due to turbine overspeeding, the safety valve position is controlled as

$$u_{safety} = \begin{cases} 1\,\text{(normal mode)} & \text{if } \Omega < \Omega^{max}, \\ 0\,\text{(safety mode)} & \text{else.} \end{cases} \tag{29}$$

It is interesting to note that the safety valve at Mutriku is electrically activated with gravity closing [24] and, therefore, if power grid connection fails, the valve automatically closes.

3.4. Methodology

For each possible combination of d_r and d_{bypass}/d_r in the parametric space (110 cases), the control system is designed, as detailed in Section 3.3, and numerical simulations are run to compute E_{elec}^{life}, therefore calculating LCoE*. To obtain E_{elec}^{life}, a lifetime of 25 years is assumed [32], and the produced annual electric energy at Mutriku is computed. To this end, 15 realisations of 20 min each are run for 58 different irregular sea states, generated from JONSWAP spectral density functions [50] with peak shape parameter $\gamma^J = 3.3$. The significant wave height, H_s, and peak period, T_p, are selected considering the characteristic wave climate measured at the Mutriku power plant [51], detailed in Fig. 9. To take into account the shoaling effect, characterising the ocean waves at Mutriku, the JONSWAP spectra are modified using an attenuation function, as detailed in [11]

In addition to LCoE*, another performance indicator, namely the capacity factor, ζ, is also computed for all the 110 combinations in the parametric space.

In the simulation, some simplifications are adopted. Since the typical bypass valve actuation time (~10 s) [32] is much lower than the typical timescale over which the sea condition changes (from 30 min to 3 h) [52], the bypass valve actuation system dynamic is ignored. Furthermore, full knowledge of the SS is assumed in this paper, although online SS estimation techniques [53] can be used in practice. Recent advances in meteorological modelling also allows wave spectra to be forecast [54]. Finally, no interruption to power production (which may be due to planned maintenance or a system failure) over the OWC lifetime is currently considered.

Table 1
OWC model parameters (MP) [11,24,32].

MP	Value	Unit	MP	Value	Unit
m_p	27 748	(kg)	$A(\infty)$	71 618	(kg)
I^{mtrk}	3.06	(kg m^2)	S_w	19.35	(m^2)
d_r^{mtrk}	0.75	(m)	ι	4.5	(m)
κ	0.775	(–)	V_0	144	(m^3)
d_r^{pico}	2.3	(m)	t_h	0.005	(m)

Table 2
Cost-related parameters (CP) [21,43,55].

CP	Value	Unit	CP	Value	Unit
b	0.45	(–)	β	2/3	(–)
μ	2.5	(–)	C_{mech}^{pico}	302.6	(k$)
C_{steel}	2.1	($/kg)	ρ_{steel}	7750	(kg/m^3)

4. Results and discussion

In this section, results are presented and discussed. Tables 1 and 2 report, respectively, the OWC model parameters, and cost-related coefficients, considered in the simulation.

As already mentioned, in this study, a parametric CCD approach is taken. In comparison with a numerical optimisation method, the parametric approach provides knowledge of the performance function across the full parametric space, therefore allowing a more comprehensive analysis into the effect of peak-shaving control on the LCoE. To simplify the discussion, a point in the parametric space will be addressed as Γ_i^j, where $i = d_r \times 100$ and $j = (d_{bypass}/d_r) \times 100$. For instance, Γ_{55}^{15} is the case in which $d_r = 0.55$ m and $d_{bypass}/d_r = 0.15$.

4.1. Result of the simulation

Figs. 10 and 11 show, respectively, LCoE*(Γ_i^j) and $\zeta(\Gamma_i^j)$. For clarity, the vertical axis in Fig. 10 is reversed. Furthermore, Fig. 12 focuses on LCoE*, and/or ζ, for some significant combinations of d_r and d_{bypass}/d_r.

Finally, Fig. 13 provides an insight into the effect of peak-shaving control, for each SS, for the case in which LCoE* is minimal (i.e., Γ_{55}^{15}). In particular, Figs. 13(c) and 13(d) show, respectively, how ζ and LCoE* vary for Γ_{55}^{15} in comparison with Γ_{55}^{0} (i.e., same d_r but no bypass valve). To analyse the variation in LCoE* for each SS, the LCoE enhancement index (LEI), is introduced, as

$$\text{LEI} = 1 - \frac{\text{LCoE}^*(\Gamma_{55}^{15})}{\text{LCoE}^*(\Gamma_{55}^{0})}, \text{ with LEI} \leq 1. \tag{30}$$

Fig. 13(d) shows the LEI for each SS and,

$$\text{if } \begin{cases} \text{LEI} = 1, & \text{LCoE}^*(\Gamma_{55}^{0}) = \infty; \\ 0 < \text{LEI} < 1, & \text{LCoE}^*(\Gamma_{55}^{15}) < \text{LCoE}^*(\Gamma_{55}^{0}); \\ \text{LEI} = 0, & \text{LCoE}^*(\Gamma_{55}^{15}) = \text{LCoE}^*(\Gamma_{55}^{0}); \\ \text{LEI} < 0, & \text{LCoE}^*(\Gamma_{55}^{15}) > \text{LCoE}^*(\Gamma_{55}^{0}). \end{cases} \tag{31}$$

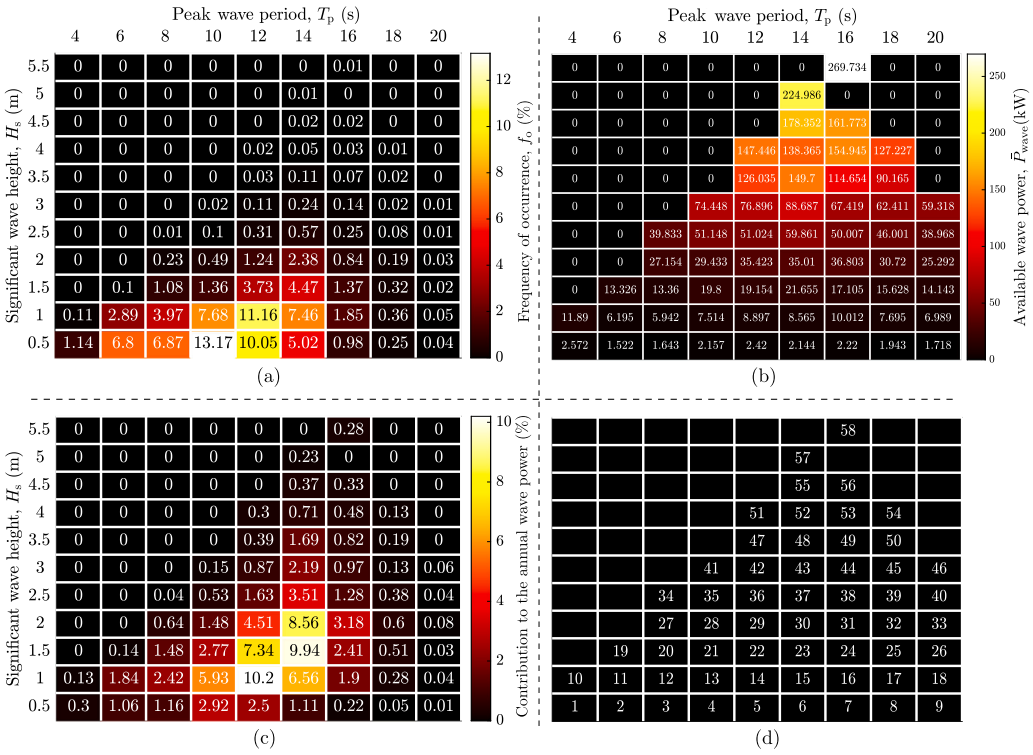

Fig. 9. Annual wave climate at Mutriku. The four scatter plots show, for each combination of H_s and T_p, (a) the frequency of occurrence (over a year) of a specific sea state at Mutriku, (b) the mean available wave power, $\bar{P}_{wave}$, (c) the contribution (specified as a percentage) of each irregular sea state to the total annual wave power available at Mutriku, and (d) the number (from 1 to 58) assigned at each irregular sea state considered in this paper.

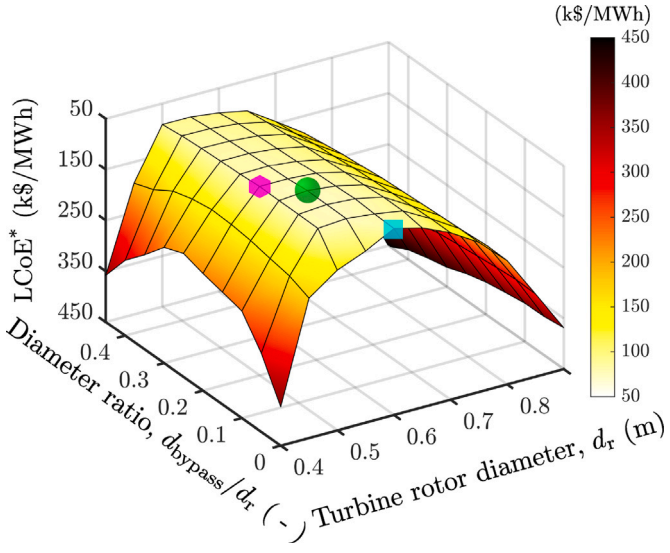

Fig. 10. LCoE* obtained from all the considered combinations of d_r and d_{bypass}/d_r. The green circle (● at Γ_{55}^{15}) highlights the condition for which LCoE* is minimised, the blue square (■ at Γ_{60}^{0}) indicates the point at which the minimum LCoE* is achieved without using a bypass valve, and the magenta hexagon (● at Γ_{50}^{20}) shows the condition for which the maximum capacity factor, ζ^{max}, is found.

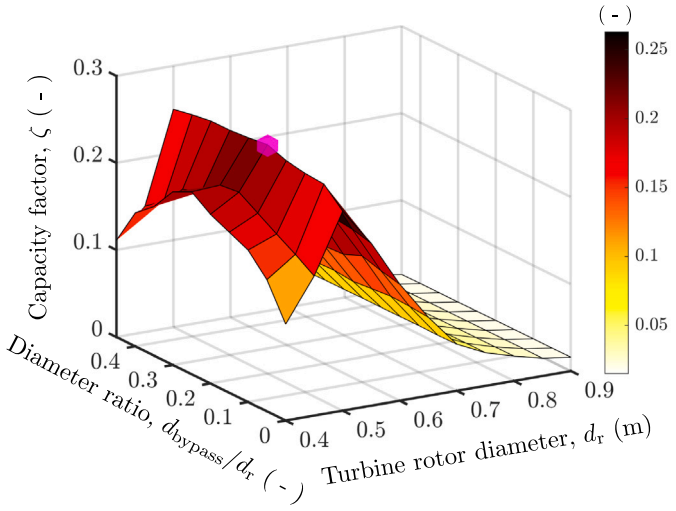

Fig. 11. Average annual value of the capacity factor, ζ, for each combination of turbine rotor diameter, d_r, and diameter ratio, d_{bypass}/d_r. The magenta hexagon (● at Γ_{50}^{20}) shows the condition for which the peak value of ζ, $\zeta^{max} = 0.263$, is achieved.

In general, LEI is expected to be larger (see Eq. (31)) in relatively high energy sea states, since rated power control plays a more important role as the available wave power increases.

4.2. Discussion

From Fig. 10, LCoE* is, unsurprisingly, more sensitive to d_r, rather than to d_{bypass}/d_r. Indeed, since the bypass valve is exclusively used for peak-shaving control, and since C_{bypass} is only a small fraction of CapEx, E_{elec}^{life} and CapEx are mainly affected by the turbine performance and size. However, if $d_r \leq 0.45$ m, the sensitivity of LCoE* to d_{bypass}/d_r increases. This is due to the fact that, for $d_r \leq 0.45$ m, the impact of peak-shaving control on E_{elec}^{life} is more significant, as it notably extends the operating range of small turbines (with lower P^{rated}). If $d_r = 0.90$ m, P^{rated} is relatively high and, therefore, LCoE* increases with d_{bypass}/d_r, as the small improvement in E_{elec}^{life} obtained with peak-shaving is not worth the additional cost of the bypass valve. It should be also noted that, if $d_{bypass}/d_r = 0$, LCoE* is minimised for $d_r = 0.60$ m whereas, if peak-shaving is used, LCoE* is minimised by a smaller (and cheaper)

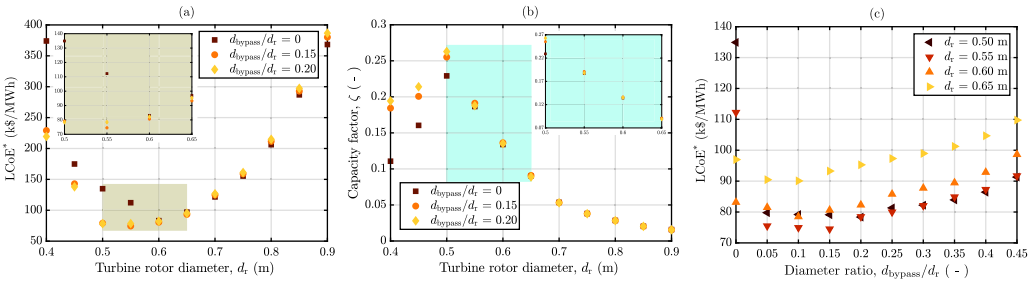

Fig. 12. LCoE* and/or capacity factor, ζ, for some significant combinations of d_r and/or d_{bypass}/d_r.

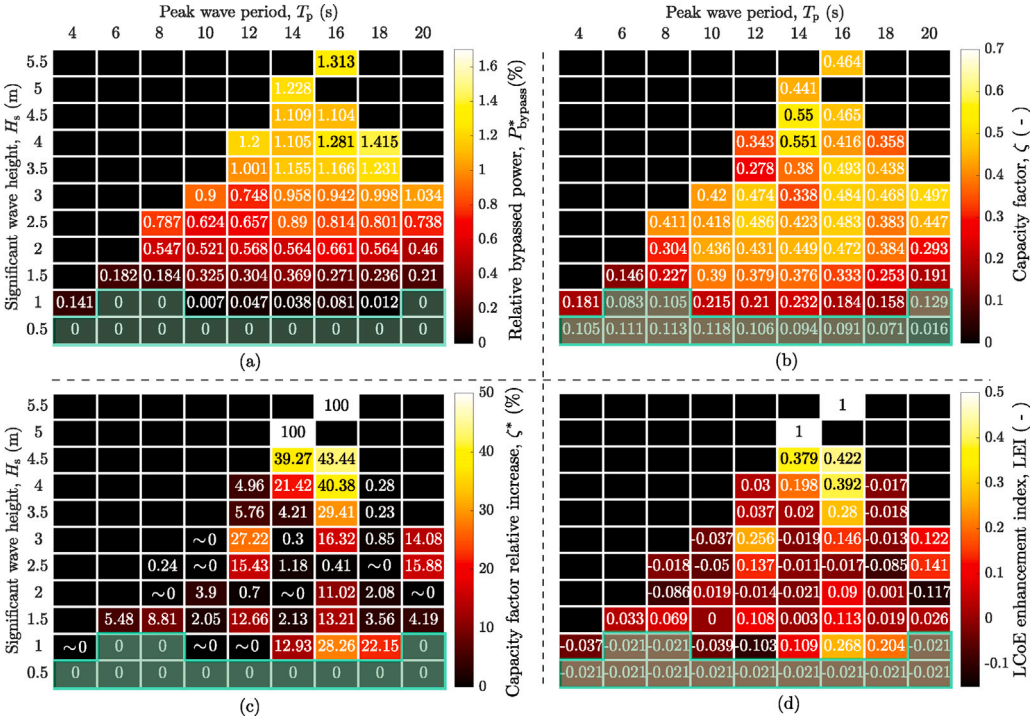

Fig. 13. Insight into the effect of the bypass valve for Γ_{55}^{15} (and Γ_{55}^{0}). The green shaded areas highlight the sea states for which the bypass valve is closed ($u_{bypass} = 0$), since $\bar{P}_{wave} \leq \bar{P}^{thr}_{wave}$, meaning that pneumatic power is not dissipated. For each combination of H_s and T_p, the four scatter plots show: (a) the relative bypassed pneumatic power, P^*_{bypass}, for Γ_{55}^{15}; (b) the capacity factor, ζ, for Γ_{55}^{15}; (c) the relative percentage increase in ζ, ζ^*, obtained for Γ_{55}^{15} in comparison with Γ_{55}^{0}; (d) the LCoE enhancement index, LEI, as defined in Eqs. (30) and (31).

turbine, with $d_r = 0.55$ m. Hypothetically, if Ω^{max}_{gen} is lower than 400 rad/s, LCoE* minimisation may suggest a larger d_r, since small turbines work efficiently only at relatively high Ω.

Ultimately, the selection of d_r is critical for minimising LCoE*, especially if $d_{bypass}/d_r = 0$. However, if $0.05 \leq d_{bypass}/d_r \leq 0.45$, a relatively flat low-valued region of LCoE* appears for $0.50 \leq d_r \leq 0.65$ m (see Fig. 11 and Figs. 12(a) and (c)). Therefore, if a bypass valve is provided, it is somewhat easier to achieve a 'close-to-minimum' LCoE* condition, as the selection of d_r becomes less critical.

Although LCoE is the objective function of the CCD approach, since peak-shaving control aims to maximise ζ, it is also worth considering ζ (see Figs. 11 and 12(b)). Although a large ζ is desirable, the minimum LCoE* (at Γ_{55}^{15}) is not equivalent to the maximum ζ (at Γ_{50}^{20}), meaning that having $\zeta = \zeta^{max} = 0.263$ does not guarantee the best return on investment. Similarly to LCoE*, ζ is more sensitive to d_r than to d_{bypass}/d_r and, furthermore, the sensitivity of ζ to d_{bypass}/d_r increases if $d_r \leq 0.45$ m.

Fig. 13 provides insight into the impact of peak-shaving control, for each SS, considering Γ_{55}^{15} and Γ_{55}^{0}. Firstly, Figs. 13(a) and (b) show, respectively, the percentage of bypassed pneumatic power, defined as

$$P^*_{bypass} = \frac{P_{bypass}}{P_{bypass} + P_{pneu}} \times 100, \tag{32}$$

and ζ, for Γ_{55}^{15}. Clearly, if $u_{bypass} = 0$, $P^*_{bypass} = 0$ (there is no power dissipation). Secondly, Fig. 13(c) shows the relative increase in capacity factor, computed as

$$\zeta^* = \frac{\zeta(\Gamma_{55}^{15}) - \zeta(\Gamma_{55}^{0})}{\zeta(\Gamma_{55}^{15})} \times 100. \tag{33}$$

Similarly to P^*_{bypass}, if $u_{bypass} = 0$, $\zeta^* = 0$. Sea states 57 and 58 have $\zeta^* = 100$, meaning that, unless a bypass valve is equipped, the OWC with $d_r = 0.55$ m stays (almost) permanently in safety mode, i.e., $\zeta(\Gamma_{55}^{0}) \sim 0$. For some SSs, $\zeta^* \sim 0$, hence peak-shaving control is neither improving nor deteriorating the capacity factor. This is arguably due to the fact that wave energy is typically characterised by a high peak-to-average power ratio and, furthermore, u_{bypass} is SS-based. Therefore, there are time periods over which power dissipation is not needed (since P_{pneu} is low), yet the bypass valve is dissipating pneumatic power. Wave-by-wave u_{bypass} control could potentially offer a more appropriate control solution but, with currently available actuators, real-time wave-by-wave control of u_{bypass} is not feasible [10,32]. In addition to the relatively high capital cost of a suitable real-time actuator, it is also likely that significant parasitic power would be consumed by such an actuator. Finally, Fig. 13(d) shows the LEI, introduced in Eqs. (30)

and (31). It should be noted that the ratio of $C_{\text{mov}}(\Gamma_{55}^{0})$ to $C_{\text{mov}}(\Gamma_{55}^{15})$ is 0.9793. Therefore, for the bypass valve at Γ_{55}^{15} to be economically beneficial (i.e., LEI > 0), peak shaving control should increase the produced electric energy by *at least*, a factor of 1.0211. In other words, the extra wave energy extractable thanks to peak-shaving control, should (at the very least) counterbalance the cost of the bypass valve.

5. Conclusions

In light of the discussion in Section 4, CCD is essential to minimise the LCoE, since the control possibilities, such as peak-shaving control, impact costs and $E_{\text{elec}}^{\text{life}}$. Furthermore, although ζ maximisation is not the final objective, it is important to increase ζ in WECs, especially if WECs are to compete against wind energy. For instance, for the Mutriku OWC, the annual mean ζ is $\sim$ 0.11 [56] while, for European wind turbines, the annual mean ζ is around 0.21–0.29 [57,58]. Thanks to the availability of suitable actuators (i.e., a bypass valve) and CCD (to find the optimum control-informed system parameters), there is certainly a significant margin for improvement in ζ for OWC WECs, as suggested by Fig. 11.

A CCD approach may have two main issues: CCD may be computationally expensive and, potentially, complex to automate. To this end, one of the main achievements of this paper is the fact that the considered CCD approach is relatively computationally friendly and straightforward to automate. First, the control system design procedure (in Section 3.3) is simple (for instance, u_{bypass} is fully determined by simply choosing $\bar{P}_{\text{wave}}^{\text{thr}}$, $\bar{P}_{\text{wave}}^{\text{max}}$, and f_{bypasss}). Indeed, keeping the control design sufficiently simple is an essential requirement to easily automate the CCD procedure. More sophisticated control strategies can always be designed later for the parametric points in the neighbourhood of the LCoE* minimum (which provides an informed initial guess obtained with the simple controllers). Furthermore, since u_{bypass} is SS-based, not all the sea states have to be simulated, for all the $\Gamma_{\text{i}}^{\text{j}}$. For a SS in which $\bar{P}_{\text{wave}} \leq \bar{P}_{\text{wave}}^{\text{thr}}$, the produced electric energy stays the same with, or without, the bypass valve. Therefore, only the SSs for which $u_{\text{bypass}} \neq 0$ have to be re-simulated. Finally, since a parametric CCD approach is considered, and since the solution for each case is independent of the other cases, different cases can run in parallel [59].

The LCoE*, in Fig. 10, provides a quantitative estimate of how much the LCoE is potentially reduced if the OWC parameters are optimised considering control. However, LCoE* likely underestimates LCoE since: (i) C_{pto} does not include cost of development and design [43], (ii) losses in the power train, such as hydrodynamic viscous losses due to vortex shedding [60], are not considered [61], (iii) even with maintenance, the OWC performance will deteriorate with age [62], and (iv) power production may be interrupted for maintenance or a system failure. In relation to (iv), if maintenance is scheduled at a convenient time (i.e., in low energy sea states), and if fault-tolerant control is used to improve maintenance operation flexibility, the increase in LCoE due to operation interruptions may be limited. In any case, the main scope of this paper is not to accurately estimate LCoE, rather to devise an automatable CCD procedure, with a reasonable computational cost, for an OWC with rotational speed and power dissipation control possibilities.

Finally, it should not be forgotten that, despite LCoE being a suitable high-level cost function, LCoE is only a statistical metric characterising the cost of the produced energy, and therefore does not fully represent the 'real value' of wave energy. For instance, the LCoE does not consider real-time factors (such as real-time energy market price/demand in relation to the availability of wave energy and/or energy from other renewable resources), energy storage (possibility to store energy and use it when required), complementarity between wave energy and other renewable resources, and the creation of job opportunities.

CRediT authorship contribution statement

Marco Rosati: Conceptualization, Methodology, Software, Validation, Writing – original draft, Visualization. **John V. Ringwood:** Supervision, Conceptualization, Methodology, Writing – review & editing.

Declaration of competing interest

The authors declare the following financial interests/personal relationships which may be considered as potential competing interests: Marco Rosati reports financial support was provided by Science Foundation Ireland.

Acknowledgements

This study was supported by MaREI, the SFI Research Centre for Energy, Climate and Marine, Ireland, under grant No. 12/RC/2302_P2. The authors want to thank Hafiz Ahsan Said and Augusto Conrado Sarda for useful technical discussions.

References

[1] B. Reguero, I. Losada, F. Méndez, A global wave power resource and its seasonal, interannual and long-term variability, Appl. Energy 148 (2015) 366–380.
[2] S. Astariz, G. Iglesias, The economics of wave energy: A review, Renew. Sustain. Energy Rev. 45 (2015) 397–408.
[3] X. Li, Diversification and localization of energy systems for sustainable development and energy security, Energy Policy 33 (17) (2005) 2237–2243.
[4] J. Widén, N. Carpman, V. Castellucci, D. Lingfors, J. Olauson, F. Remouit, M. Bergkvist, M. Grabbe, R. Waters, Variability assessment and forecasting of renewables: A review for solar, wind, wave and tidal resources, Renew. Sustain. Energy Rev. 44 (2015) 356–375.
[5] F. Fusco, G. Nolan, J.V. Ringwood, Variability reduction through optimal combination of wind/wave resources – An Irish case study, Energy 35 (1) (2010) 314–325.
[6] A.F.O. Falcão, J.C.C. Henriques, Oscillating-water-column wave energy converters and air turbines: A review, Renew. Energy 85 (2016) 1391–1424.
[7] A.F.O. Falcão, L.C. Vieira, P.A.P. Justino, J.M.C.S. André, By-pass air-valve control of an OWC wave power plant, J. Offshore Mech. Arct. Eng. 125 (3) (2003) 205–210.
[8] K. Monk, V. Winands, M. Lopes, Chamber pressure skewness corrections using a passive relief valve system at the Pico oscillating water column wave energy plant, Renew. Energy 128 (2018) 230–240.
[9] A.F.O. Falcão, L.M.C. Gato, Air turbines, in: A. Sayigh (Ed.), Comprehensive Renewable Energy, Vol. 8, Elsevier, Oxford, 2012, pp. 111–149.
[10] M. Rosati, J.V. Ringwood, J.C.C. Henriques, A comprehensive wave-to-wire control formulation for oscillating water column wave energy converters, Trends Renew. Energy Offshore (2022) 329–337.
[11] J.C.C. Henriques, J.C.C. Portillo, W. Sheng, L.M.C. Gato, A.F.O. Falcão, Dynamics and control of air turbines in oscillating-water-column wave energy converters: Analyses and case study, Renew. Sustain. Energy Rev. 112 (2019) 571–589.
[12] D.L. O'Sullivan, A.W. Lewis, Generator selection and comparative performance in offshore oscillating water column ocean wave energy converters, IEEE Trans. Energy Convers. 26 (2) (2011) 603–614.
[13] S. Astariz, A. Vazquez, G. Iglesias, Evaluation and comparison of the levelized cost of tidal, wave, and offshore wind energy, J. Renew. Sustain. Energy 7 (5) (2015).
[14] G. Chang, C.A. Jones, J.D. Roberts, V.S. Neary, A comprehensive evaluation of factors affecting the levelized cost of wave energy conversion projects, Renew. Energy 127 (2018) 344–354.
[15] B. Guo, J.V. Ringwood, Geometric optimisation of wave energy conversion devices: A survey, Appl. Energy 297 (2021) 117100.
[16] P.B. Garcia-Rosa, G. Bacelli, J.V. Ringwood, Control-informed geometric optimization of wave energy converters: The impact of device motion and force constraints, Energies 8 (12) (2015) 13672–13687.
[17] J.T. Allison, D.R. Herber, Special section on multidisciplinary design optimization: Multidisciplinary design optimization of dynamic engineering systems, AIAA J. 52 (4) (2014) 691–710.
[18] H.K. Fathy, J.A. Reyer, P.Y. Papalambros, A. Ulsov, On the coupling between the plant and controller optimization problems, in: Proc. of the 2001 American Control Conference.(Cat. No. 01CH37148), Vol. 3, IEEE, 2001, pp. 1864–1869.
[19] C.A.M. Ströfer, D.T. Gaebele, R.G. Coe, G. Bacelli, Control co-design of power take-off systems for wave energy converters using WecOptTool, IEEE Trans. Sustain. Energy (2023) 1–11.
[20] G. Bacelli, R.G. Coe, Comments on control of wave energy converters, IEEE Trans. Control Syst. Technol. 29 (1) (2021) 478–481.
[21] Y. Peña-Sanchez, D. García-Violini, J.V. Ringwood, Control co-design of power take-off parameters for wave energy systems, IFAC-PapersOnLine 55 (27) (2022) 311–316, 9th IFAC Symposium on Mechatronic Systems.
[22] M. Garcia-Sanz, Control co-design: an engineering game changer, Adv. Control Appl. Eng. Ind. Syst. 1 (1) (2019) e18.

[23] M. Rosati, J.V. Ringwood, Wave-to-wire efficiency maximisation for oscillating water column systems, in: Proc. of the 22nd IFAC World Congress, International Federation of Automatic Control, Yokohama, Japan, 2023.
[24] Y. Torre-Enciso, I. Ortubia, L.I.L. De Aguileta, J. Marqués, Mutriku wave power plant: From the thinking out to the reality, in: Proc. of the 8th European Wave and Tidal Energy Conference, Uppsala, Sweden, 2009, pp. 319–329.
[25] M. Rosati, J.C.C. Henriques, J.V. Ringwood, Oscillating-water-column wave energy converters: A critical review of numerical modelling and control, Energy Convers. Manage. X 16 (2022) 100322.
[26] J.M. Silva, S.M. Vieira, D. Valério, J.C.C. Henriques, GA-optimized inverse fuzzy model control of OWC wave power plants, Renew. Energy 8 (2023) 17–29.
[27] M. Rosati, H.A. Said, J.V. Ringwood, Wave-to-wire control of an OWC wave energy system equipped with a wells turbine, 2023.
[28] J.C.C. Henriques, L.M.C. Gato, J.M. Lemos, R.P.F. Gomes, A.F.O. Falcão, Peak-power control of a grid-integrated oscillating water column wave energy converter, Energy 109 (2016) 378–390.
[29] A.A.D. Carrelhas, L.M.C. Gato, J.C.C. Henriques, Peak shaving control in OWC wave energy converters: From concept to implementation in the Mutriku wave power plant, Renew. Sustain. Energy Rev. 180 (2023) 113299.
[30] F. Paparella, K. Monk, V. Winands, M.F.P. Lopes, D. Conley, J.V. Ringwood, Up-wave and autoregressive methods for short-term wave forecasting for an oscillating water column, IEEE Trans. Sustain. Energy 6 (1) (2015) 171–178.
[31] C. Roh, Enhancing power generation stability in oscillating-water-column wave energy converters through deep-learning-based time delay compensation, Processes 11 (6) (2023) 1787.
[32] A.F.O. Falcão, A.J.N.A. Sarmento, L.M.C. Gato, A. Brito-Melo, The Pico OWC wave power plant: Its lifetime from conception to closure 1986–2018, Appl. Ocean Res. 98 (2020) 102104.
[33] D.V. Evans, The oscillating water column wave-energy device, IMA J. Appl. Math. 22 (4) (1978) 423–433.
[34] J. Falnes, Wave interaction with oscillating water columns, in: Ocean Waves and Oscillating Systems, Cambridge University Press, 2002, pp. 225–262.
[35] J.N. Ewman, C.H. Lee, WAMIT User Manual, 2016, URL http://www.wamit.com/manual.htm. (Last accessed 02 March 2019).
[36] W. Sheng, R. Alcorn, A. Lewis, A new method for radiation forces for floating platforms in waves, Ocean Eng. 105 (2015) 43–53.
[37] T. Kelly, Experimental and Numerical Modelling of a Multiple Oscillating Water Column Structure (Ph.D. thesis), National University of Ireland Maynooth, 2018.
[38] A.F.O. Falcão, J.C.C. Henriques, The spring-like air compressibility effect in OWC wave energy converters: Hydro-, thermo-and aerodynamic analyses, in: International Conference on Offshore Mechanics and Arctic Engineering, American Society of Mechanical Engineers, Madrid, Spain, 2018.
[39] S.L. Dixon, C. Hall, Fluid Mechanics and Thermodynamics of Turbomachinery, Butterworth-Heinemann, 2013.
[40] M. Rosati, J.V. Ringwood, Towards hydrodynamic control of an oscillating water column wave energy converter, Trends Renew. Energy Offshore (2022) 411–418.
[41] L.M.C. Gato, A.A.D. Carrelhas, J.C.C. Henriques, Turbine-Generator Set Laboratory Tests in Variable Unidirectional Flow, Tech. Rep., OPERA - Open Sea Operating Experience to Reduce Wave Energy Costs, Deliverable D3.2, 2017.
[42] K.M. Nielsen, T.S. Pedersen, P. Andersen, S. Ambühl, Optimizing control of wave energy converter with losses and fatigue in power take off, IFAC-PapersOnLine 50 (1) (2017) 14680–14685.
[43] A.F.O. Falcão, Stochastic modelling in wave power-equipment optimization: maximum energy production versus maximum profit, Ocean Eng. 31 (11) (2004).
[44] M. Takao, K. Itakura, T. Setoguchi, T.H. Kim, K. Kaneko, M. Inoue, Noise characteristics of turbines for wave power conversion, in: Proceedings of the Eleventh International Ocean and Polar Engineering Conference, Stavanger, Norway, 2001.
[45] J.C.C. Henriques, L.M.C. Gato, V. La Sala, A.A.D. Carrelhas, Acoustic noise emission of air turbines for wave energy conversion: Assessment and analysis, Renew. Energy 212 (2023) 897–907.
[46] J. Falnes, et al., Optimum control of oscillation of wave-energy converters, in: The Eleventh International Offshore and Polar Engineering Conference, International Society of Offshore and Polar Engineers, Stavanger, Norway, 2001.
[47] A.J. Garrido, I. Garrido, M. Amundarain, M. Alberdi, M. De la Sen, Sliding-mode control of wave power generation plants, IEEE Trans. Ind. Appl. 48 (6) (2012) 2372–2381.
[48] F.M. Strati, G. Malara, F. Arena, Performance optimization of a U-oscillating-water-column wave energy harvester, Renew. Energy 99 (2016) 1019–1028.
[49] D. García-Violini, Y. Peña-Sanchez, N. Faedo, F. Ferri, J.V. Ringwood, A broadband time-varying energy maximising control for wave energy systems (LiTe-Con+): Framework and experimental assessment, IEEE Trans. Sustain. Energy (2023) 1–10.
[50] K. Hasselmann, T.P. Barnett, E. Bouws, H. Carlson, D.E. Cartwright, K. Enke, J.A. Ewing, A. Gienapp, D.E. Hasselmann, P. Kruseman, et al., Measurements of wind-wave growth and swell decay during the joint north sea wave project (JONSWAP), Deutches Hydrogr. Inst. (1973).
[51] A.A.D. Carrelhas, L.M.C. Gato, Reliable control of turbine–generator set for oscillating-water-column wave energy converters: Numerical modelling and field data comparison, Energy Convers. Manage. 282 (2023) 116811.
[52] Y. Peña-Sanchez, A. Mérigaud, J.V. Ringwood, Short-term forecasting of sea surface elevation for wave energy applications: The autoregressive model revisited, IEEE J. Ocean. Eng. 45 (2) (2020) 462–471.
[53] H. Majidian, L. Wang, H. Enshaei, Part. A: A review of the real-time sea-state estimation, using wave buoy analogy, Ocean Eng. 266 (2022) 111684.
[54] P.A.E.M. Janssen, Progress in ocean wave forecasting, J. Comput. Phys. 227 (7) (2008) 3572–3594.
[55] G. Laface, Productivity Analysis of Different Design for OWC Nearshore in Breakwater in Pantelleria (Master's thesis), Politecnico di Torino, Turin, Italy, 2021.
[56] G. Ibarra-Berastegi, J. Sáenz, A. Ulazia, P. Serras, G. Esnaola, C. Garcia-Soto, Electricity production, capacity factor, and plant efficiency index at the Mutriku wave farm (2014–2016), Ocean Eng. 147 (2018) 20–29.
[57] N. Boccard, Capacity factor of wind power realized values vs. estimates, Energy Policy 37 (7) (2009) 2679–2688.
[58] F. Monforti, M. Gaetani, E. Vignati, How synchronous is wind energy production among European countries? Renew. Sustain. Energy Rev. 59 (2016) 1622–1638.
[59] R. Oberdieck, E.N. Pistikopoulos, Parallel computing in multi-parametric programming, in: Z. Kravanja, M. Bogataj (Eds.), Computer Aided Chemical Engineering, in: 26 European Symposium on Computer Aided Process Engineering, vol. 38, Elsevier, 2016, pp. 169–174.
[60] A. Çelik, An experimental investigation into the effects of front wall geometry on OWC performance for various levels of applied power take off dampings, Ocean Eng. 248 (2022) 110761.
[61] A.F.O. Falcão, Control of an oscillating-water-column wave power plant for maximum energy production, Appl. Ocean Res. 24 (2) (2002) 73–82.
[62] D.L. Bruschi, J.C.S. Fernandes, A.F.O. Falcão, C.P. Bergmann, Analysis of the degradation in the Wells turbine blades of the Pico oscillating-water-column wave energy plant, Renew. Sustain. Energy Rev. 115 (2019) 109368.